Molecular Composites Comprising TiO_2 and Their Optical Properties

YuanQiao Rao* and Samuel Chen

Eastman Kodak Company, 1999 Lake Avenue, Rochester, New York 14650-2109

Received February 19, 2008; Revised Manuscript Received April 26, 2008

ABSTRACT: An *in situ* synthesis to form an organic−inorganic hybrid film with tunable optical properties is described. The nanocomposite comprises a titania nanophase that is formed from titanium alkoxide in the presence of a matrix polymer. XPS study indicates that titanium (Ti) in the nanophase is fully oxidized to Ti(IV), similar to that in TiO_2. When a random copolymer, of styrene and 3-methacryloxypropyltrimethoxysilane (MPTMS), comprising functional groups that form a covalent bond with the *in situ* synthesized TiO_2 is used, TEM and AFM show no phase contrast between the organic and inorganic phases at the nanometer level. This suggests a molecular level mixing of the polymer and formed inorganics and thus the formation of a molecular composite. This synthesis generates transparent composite films with any level of incorporation of TiO_2. The refractive indices of these molecular composite films are much higher than that predicted on the basis of effective medium theories; e.g., at a TiO_2 loading of 27 vol %, the resulting molecular composite film exhibits a measured refractive index of 1.76 compared to that of 1.66 predicted by effective medium theories.

Introduction

Optical material is expected to play a key role as the functional material for future information technology (IT). Computers are beginning to work in the nanosecond time scale for logic operations and in picoseconds for switching gates in microprocessor chips. Yet a faster medium is still missing for the mounting and micropackaging processes, all of which likely will be based on light optics in future generation IT components. In addition, optical material is in great demand for optical fibers, display films, and lenses. These trends clearly point to the imminent need for new optical materials.

Nanocomposites have attracted considerable attention in recent years. Most reports make use of nanodimension-defined properties to produce novel and unique applications,[1,2] as these modified materials can provide characteristics suitable for standalones as well as improvements in properties relating to strength, durability, and processability.[3] One of the challenges of creating composite materials for optical applications is the requirement to retain transparency. Scattering control at different length scale is critical for different applications. In some applications, e.g. lenses, the material needs to be transparent to the human eye, and hence the dimension of the inhomogeneity needs to be less than one-tenth the wavelength of the light, i.e., ca. 50 nm.[4,5] However, in other applications, for example, information transfer, an even smaller inhomogeneity dimension is required to prevent light scattering induced signal loss, especially over long transmission distances. Raleigh scattering calculation has shown that this loss can become significant once nanoparticles exceed 10 nm, and poor size control in these materials can easily render such materials unusable.[6]

It is well-known that dispersion control of particles in nanocomposites is challenging because the functional nanoparticles tend to self-aggregate. Tremendous research effort has been devoted to stabilize and separate the nanoparticles by capping them using organic shells in order to overcome the inherent van der Waals attraction between particles.[1,7−9] Further reading is directed to the research field of colloid chemistry.[10] When encapping stabilization is used to generate nanocomposites, several problems can arise. First, the achievable morphology of the nanocomposite may be limited. Some nanocomposites can assume a dispersed nanodomain but cannot form a cocontinuous phase. Further, the organic shell used to stabilize nanoparticles usually is detrimental to the desirable function. First, it lowers the maximum loading of the nanofiller. Assuming a 2 nm thick layer is needed to protect a 5 nm sphere particle, then the shell volume is already 70% of the particle volume. Thus, a maximum filler loading of 57 vol % is possible, even without adding any matrix polymer! Second, the organic shell can be a weak link in the stability of the nanocomposites. Any significant loss of surface passivation results in particle aggregation, and the resulting light scattering can quickly render the composite unsuitable for optical application. Therefore, there is a strong need to explore new ways to generate nanocomposites. Furthermore, for optical applications, a minimization of the nanodomain is required.

Experimental Section

Synthesis of PS−MPTMS. PS−MPTMS was synthesized by the copolymerization of styrene and (methylacryloxypropyl)trimethoxysilane (MPTMS) monomers. Under argon protection, a 50 mL flask was charged with 27.5 mL of anhydrous toluene (Sigma-Aldrich), 10 g (96 mmol) of styrene (Aldrich, reagent plus), and 8.3 g (32 mmol) of MPTMS (Fluka, >95%). The solution was stirred for 5 min, and then 64 mg of 2,2′-azobis(2,4-dimethylpentanenitrile) (Aldrich) was added. The solution was then heated to 60 °C for 20 h, after which it was cooled to room temperature and precipitated into 1 L of heptane (Aldrich, >96% for HPLC). The polymer precipitate was collected by filtration, redissolved into 50 mL of toluene, and reprecipitated into 1 L of heptane. The product was washed with heptane several times and dried at 1 mTorr vacuum overnight to yield 8.5 g (46%) of dried polymer. The polymer is readily soluble in toluene, MEK, and THF. The number-average molecular weight of the polymer is around 20 000 and the M_w/M_n is around 2, according to size exclusion chromatography (SEC) measurement. The copolymer composition is PS:MPTMS = 65:35 based on NMR measurement.

Nanocomposite Film Coating. Solutions of PS, PMMA, and P(S−MPTMS) in anhydrous toluene or tetrahydrofuran (Sigma-Aldrich, >99.9% purity) were first prepared and sealed with Teflon/silicone caps. Titanium isopropoxide (TIP, $Ti[OCH(CH_3)_2]_4$, Sigma-Aldrich, 97% purity) was then added to the solution using a syringe. Here a titania precursor was kept from any hydrolysis and condensation. Usually the concentration of the solution was controlled to be 4%, with the composition of TIP controlled to be 0%, 20%, 40%, 60%, 80%, and 100%. The solution was clean and

* Corresponding author: Fax 585-477-7781; e-mail yuanqiao.rao@kodak.com.

10.1021/ma800371v CCC: $40.75
Published on Web 06/03/2008

Table 1. Summary of Compositions of Transparent Polymer−Titania Composite Films

polymer in the composite	volume fraction of TiO_2 for transparent films (vol %)	
PS	<8.6	or>64
PMMA	<2.3	or>75
PS−MPTMS	the whole range (<100)	

Table 2. Refractive Index of PS−MPTMS/TiO_2 Composite Films (Standard Deviation in Parentheses)

PS−MPTMS (vol %)	TiO_2 (vol %)	refractive index
100.0	0.0	1.54 (0)
99.0	1.0	1.56 (0.01)
97.7	2.3	1.59 (0.01)
91.4	8.6	1.65 (0.01)
87.7	12.3	1.68 (0.01)
82.1	17.9	1.70 (0.01)
72.7	27.3	1.76 (0.01)
54.3	45.7	1.84 (0.03)
36.0	64.0	1.91 (0.01)
24.8	75.2	1.94 (0.01)
9.7	90.3	1.95 (0.01)
0.0	100.0	2.0 (0)

easily filtered through 0.45 μm PTFE filters. Thin films of nanocomposites were obtained by the method of blade coating or spin coating. In the process of spin coating, the solution was poured directly onto the Si wafer carefully until it covered the whole area and a standard photoresist spinner was used to spin the substrate at speeds from 2000 to 3000 rpm. In the process of blade coating, the solution was dripped onto a PET carrier substrate and coated using a doctor blade. The humidity of the environment was controlled at 30% RH during coating. The films were then put into a humidity oven and conditioned for 2 h at 90% RH and 70 °C. Afterward, the films were annealed in a vacuum (10^{-3} Torr) at 150 °C for 30 min.

Characterization. Optical characterization was carried out using a Woolam alpha-SE spectroscopic ellipsometer and a Perkin-Elmer Lambda 2 UV/vis spectrophotometer. To successfully carry out an ellipsometer measurement, the sample coatings were made smooth and uniform. The ellipsometer-measured film thickness showed less than 0.1% thickness variation, taken from three neighboring areas of any coating. The refractive index is reported at 632.8 nm. Three samples of the same composition were prepared for refractive index measurement. The standard deviation of the refractive index is between 0.01 and 0.03, as shown in Table 2.

Surface morphology profiles of all the nanocomposite films were analyzed using a Digital Instruments Nanoscope III atomic force microscope. The microstructure of the nanocomposites was studied using microtomed cross sections in a JEM-2000FX transmission electron microscope (TEM), operating at 200 kV accelerating voltage. The chemical composition was analyzed using a Physical Electronics 5600 photoelectron spectrometer equipped with a monochromatic Al Kα X-ray (1486.6 eV) source.

Results and Discussion

In this paper, we explore a new approach, generally called *in situ* composite synthesis, to produce a novel type of organic−inorganic hybrid optical material suitable for optical applications. The synthesis strategy is to form the nanoparticle in the presence of only the matrix polymer, as shown in Figure 1. It is a solution process in which the particle precursor and polymer are first dissolved in a solvent. The combination is then cast on a substrate and dried in a controlled way before being separated from the substrate. This process needs to be carefully controlled to ensure that the synthesized particle possesses a dimension less than 10 nm. The key reactant is the nanoparticle precursor, which needs to be completely soluble in the polymer solution. It also needs to have the reactivity to easily convert into the desired nanoparticle as well as having the capability to allow functional groups to be attached on the outside of the particles to encourage interaction with the matrix polymer.

Both kinetic and thermodynamic forces control the size of the nanodomain. One control factor is the diffusion rate. It is expected that the gelation of the polymer can be used to delay the migration of the nanoparticle intermediate until the particle has solidified. The additional control factor to further improve nanoparticle dispersion is the strength of the interaction between the nanodomain surface and polymer. Figure 2 describes several possible interactions and the corresponding morphologies of the nanodomain formed using this synthesis. In situation (a), there is only weak and nonspecific interaction between the polymer and the soluble nanoparticle precursor. There is a strong tendency for the particle precursor or the intermediate to react with each other to form larger aggregates during the process of drying. But this growth can be stopped when the polymer gels upon the removal of the solvent, and the partially converted particle loses its mobility. This composite would possess a dispersed nanodomain. In situations (b) and (c), there is a specific interaction between the particle precursor and the polymer. During drying, there is competition between particle generation and interaction formation . Depending on the strength of the interaction, the precursor can either form nanoparticles with low fractal dimension (b) or be closely knit with the polymer chain (c). In situation (c), a covalent bond is formed between the metal and the polymer. This bond localizes the formed particles and results in a metal−polymer composite dispersed at the molecular level.

One type of nanoparticle precursor is metal alkoxide. The sol−gel chemistry of metal alkoxide has been studied for several decades, and its chemistry is reasonably well understood.[11] Titanium alkoxide was chosen in this study because of the interest in making high refractive index material via TiO_2. Chemically, titanium alkoxide is known to be highly reactive, and it can readily undergo hydrolysis and condensation to generate titania. In the presence of silane-based compounds, it can also form a covalent bond with silicon alkoxide.[12–14] When different polymers with varying degrees of interactions with titanium alkoxide were used (polystyrene (PS), poly(methyl methacrylate) (PMMA), and a copolymer of styrene and 3-methacryloxypropyltrimethoxysilane (PS−MPTMS), different composite morphologies were observed. Depending on the polymer and the range of composite composition, some of the formed composites were found to be transparent. The morphology of transparent composite films was examined under the TEM, and an array of microstructures was found (Figure 3). For polystyrene-based composites, the nonspecific interaction with the alkoxide group produced dispersed nanodomains with the domain size less than 100 nm (Figure 3a). For PMMA-based composites, in which hydrogen bonds can form with metal hydroxyl groups, composites comprising fractal particles were seen (Figure 3b), and the percolation threshold of such composites was found to be much lower than that based on PS. By comparison, when the polymer was a copolymer that comprised silane alkoxide (such as PS−MPTMS), there was no phase contrast seen by TEM, shown for the coating at 30 vol % TiO_2 when mixed with PS−MPTMS (Figure 3c). This indicates the absence of segregation by either the organic or inorganic phases. Under this condition, we refer to this as a molecular composite. In summary, the microstructure morphology of composite films changes with the type of polymer. This morphology directly affects the optical transparency of the composite film. As shown in Table 1, there was a maximum titania loading level in PS and PMMA below which the composite film maintains optical transparency. By contrast, the PS−MPTMS composite films were transparent for all of the compositions tested.

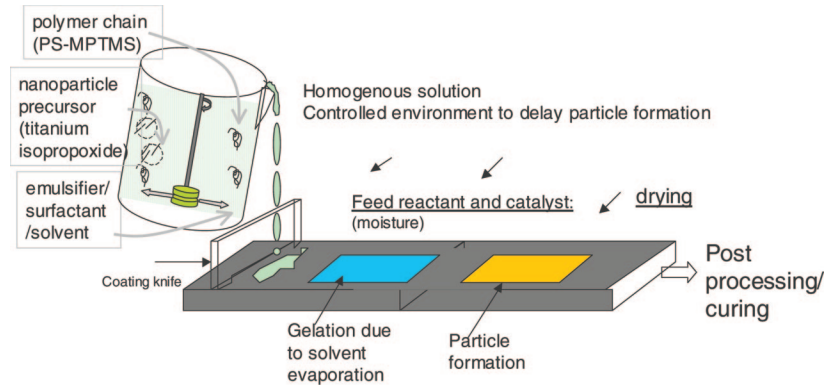

Figure 1. Schematic description of *in situ* nanocomposite synthesis.

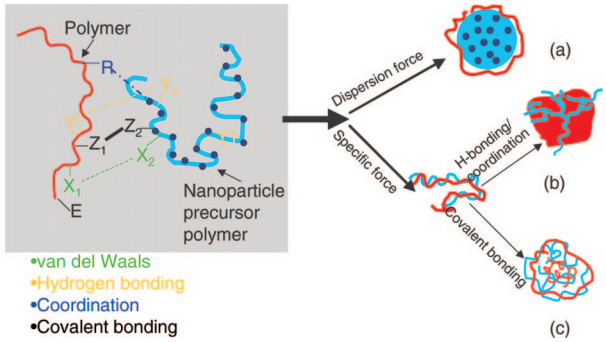

Figure 2. Schematics of size control in *in situ* composite synthesis.

Molecular composite requires the inorganic phase to be intimately mixed with the organic polymer component. While neither molecular composite nor sol−gel-based hybrid material synthesis is conceptually new, the potential of such hybrid materials has only recently been recognized, explored, and published. Notably, Manners et al. developed a class of iron-containing polymer using metal-catalyzed ring-opening polymerization.[15] One difference between the metal-containing polymer and our material is analogous to that between thermal plastics and thermosets, in which the former can easily deform at elevated temperatures. On the other hand, researchers began to work on sol−gel hybrid synthesis in 1985.[16–23] Most early work was centered around the incorporation of silica into organic materials, partially due to the limited availability of metal alkoxides.[24] The silicon-based hybrid material was usually made using organosilane alkoxide and silane alkoxide. The organic groups only embellish the silica network instead of serving as the major phase. There has been limited research on incorporating sol−gel-synthesized TiO_2 into a polymer.[25–28] These composites have limited optical applications at high TiO_2 loading because of the difficulty in controlling nanophase incorporation at the molecular level.

While the high refractive index and photocatalytic activity of TiO_2 are desirable, these properties depend on its crystalline form.[29–31] Hence, it is necessary to understand the type of TiO_2 formed in our *in situ* composite synthesis. Earlier study on sol−gel synthesis of TiO_2 using titanium alkoxide suggested that the formed TiO_2 before calcinations is amorphous.[32–37] In the present study, XPS results showed that the Ti in the composite has a similar electron environment as that in the pure sol−gel-formed TiO_2, and it is similar to TiO_2 annealed at 600 °C. For the nanocomposite, the high-resolution spectrum of the Ti 2p peak (Figure 4) showed two peaks that are consistent with anatase TiO_2, with Ti $2p_{3/2}$ at a binding energy (BE) of 459 eV and Ti $2p_{1/2}$ at BE 464.9 eV.[25,38] This suggests a successful conversion of the titanium alkoxide to TiO_2 in the presence of the polymer. Solid-state Si nuclear magnetic resonance (NMR) of the composite showed the formation of a Si−O−metal bond, indicating that titanium metal is in intimate contact with the Si containing PS−MPTMS polymer (Figure 4b).

Optical property measurement and annealing experiments were further carried out on the pure sol−gel-formed titania to understand the particle properties. The sol−gel titania film after curing at 150 °C was further heated to 300, 400, 500, 600, 700, 1000, and 1010 °C. X-ray diffraction (XRD) was used to characterize the structure of the titania films, and an ellipsometer was used to study the temperature-induced change of refractive index and film thickness. XRD results indicate the formed titania is amorphous in films processed to 150 °C, as no low angle diffraction peaks were detected. The titania film begins to crystallize at around 300 °C, and small diffraction peaks, corresponding to anatase, appear and grow with increasing temperature. There is a step change in the thickness of the film at 300 °C, suggesting densification during crystallization. The anatase polycrystalline film transforms into a more thermally stable rutile phase at about 1000 °C. At these temperatures, significant reduction in film thickness occurs, consistent with an increase in density of the rutile phase. The density of the amorphous film is calculated on the basis of thickness change to be 3.0 g cm^{-3}, and the refractive index is measured to be 2.0.

The optical properties of the composite films comprising sol−gel TiO_2 and PS−MPTMS (65% PS and 35% MPTMS as calculated from ^1H solution NMR) were examined in detail. The composite films at all compositions are optically transparent and have a measured transmission of 100% in the 400−700 nm range. Only when annealed at high temperatures to form a crystallized nano TiO_2 film was an absorption peak found at 290 nm (in the UV range). The nonabsorbing nature of the composite film was also confirmed by ellipsometry. The calculation used in our ellispometer analysis is based on Cauchy's model in which both n and k are variables. All the ellipsometer measurement gave a k value of 0, consistent with the nonabsorbing nature of the films (Figure 5b). Table 2 shows the refractive index with different volume fractions of the amorphous TiO_2. The refractive index of the PS−MPTMS is 1.54. It is known that PS has a refractive index of 1.58. The addition of the PMMA-based comonomer reduces the refractive index. It is expected that another comonomer, styrene silicon alkoxide, can be used such that the refractive index of the initial polymer is similar to that of PS. When the amount of TiO_2 is higher than 12 vol %, the refractive index increases beyond 1.68. Polymers typically have refractive indices between 1.40 and 1.67,[39] and it is difficult to make an optically transparent polymer with an index higher than 1.67. The maximum refractive index of a polymer is limited by the atoms that form the polymer, which usually contain C, H, O, and N. In order to

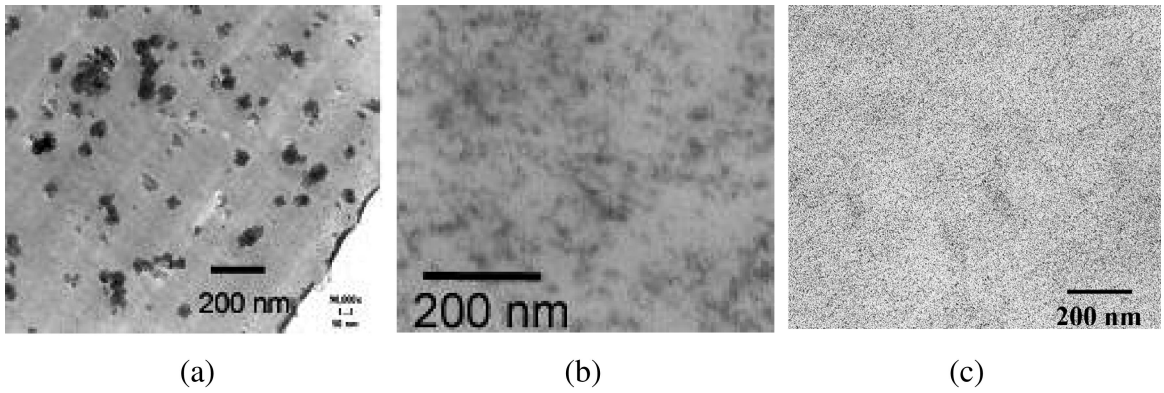

Figure 3. TEM micrographs of different TiO_2 nanocomposites: (a) polystyrene composite with 6 vol % TiO_2, (b) poly(methyl methacrylate) composite with 6 vol % TiO_2, and (c) PS−MPTMS composite with 30 vol % TiO_2.

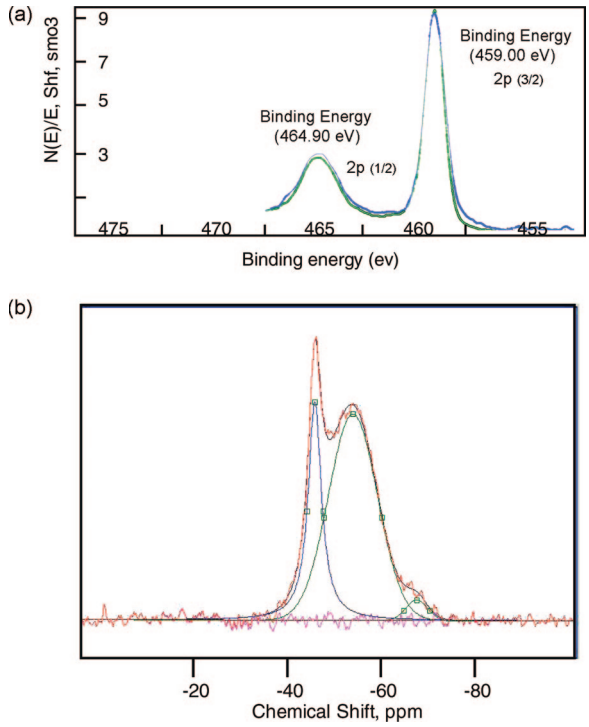

Figure 4. (a) High-resolution XPS of Ti 2p: blue trace is the composite film, and the green trace is the pure sol−gel-formed anatase titania that was further annealed at 600 °C for 1 h. (b) ^{29}Si NMR spectrum of a copolymer−TiO_2 (50 vol % TiO_2) composite film.

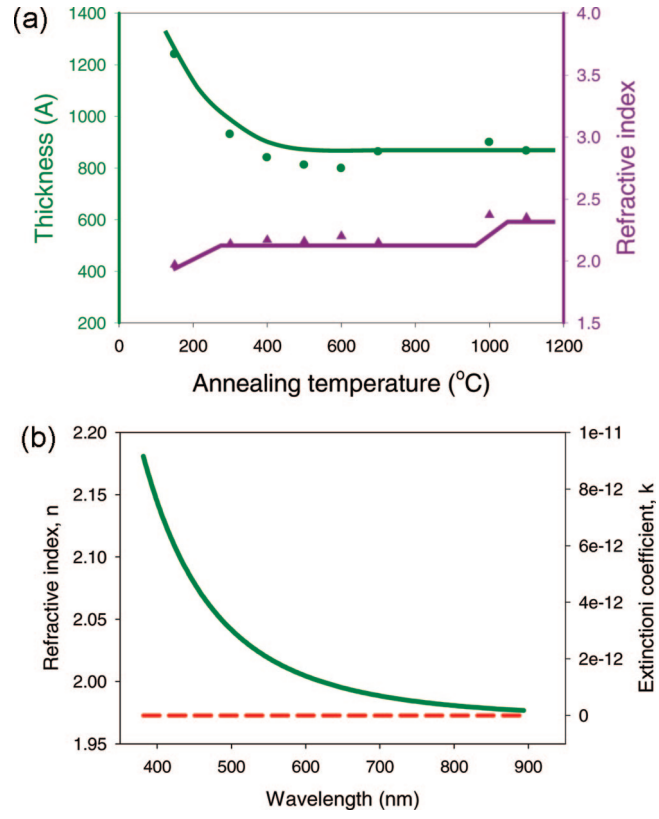

Figure 5. (a) Thickness and refractive index of the sol−gel titania film at different annealing temperatures measured by an ellipsometer: green dots are thickness, and purple triangles are refractive index at 632.8 nm. (b) Optical constant vs wavelength for 100% TiO_2 annealed at 150 °C. Solid green line represents refractive index, and dashed red line represents the extinction coefficient.

achieve a refractive index close to or higher than 1.7, a different atom with higher electron density need to be incorporated. There have been significant advances on exploring the effect of the nanodomain to adjust the refractive index of a material.[40–42] However, the optical transmission and refractive index were limited by the amount of TiO_2 that can be uniformly incorporated.

Theoretical treatment of composite refractive index has often been used to predict optical properties in composites, and a widely used method has been the effective medium models,[4] based on the Maxwell equation. These treatments realize that the response is dependent on the microstructure of the nanocomposite. The Maxwell−Garnett theory was used to model the effective electric permittivity of heterogeneous media comprising monodispersed, nanosized spheres arranged in a cubic lattice structure.[42,43] Bruggeman extended the theory to consider the polydispersed spheres or two intermixing phases.[44] Parallel and series models were derived for the refractive index of two directions when the material has two alternating parallel nanophases, confined by upper and lower limits on the composite refractive index.[40,45] del Rio et al. derived the effective dielectric properties by applying volume average theory (VAT) to the Maxwell equation.[46] There has been work that was based on the above approaches and further took into consideration particle shapes.[47,48] In addition to analytical treatments, numerical simulation was also used and shown to have good agreement with the VAT model.[49] Experimentally, different composite materials were found to follow the predictions of the series model or the Maxwell−Garnett treatment, and generally their refractive index falls between the upper and lower bound of the different models. To visualize the effect of filler volume on refractive index, Figure 6 plots the predicted value with the volume fraction of filler for different models.

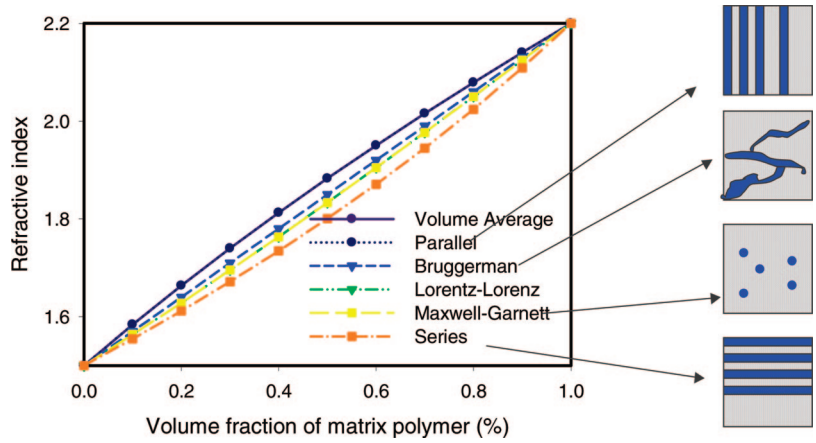

Figure 6. Composite refractive index vs the volume fraction of high index component assuming that the low index material has a refractive index of 1.5 and the high index material has a refractive index of 2.2.

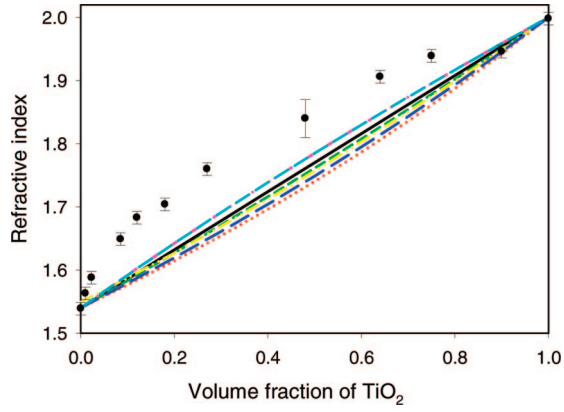

Figure 7. Experimental composite refractive index vs model predicted values at different high index material loading. The dot represents the experimental data with the error bar; the lines of different colors represent the model prediction using different theories based on the effective media theories.

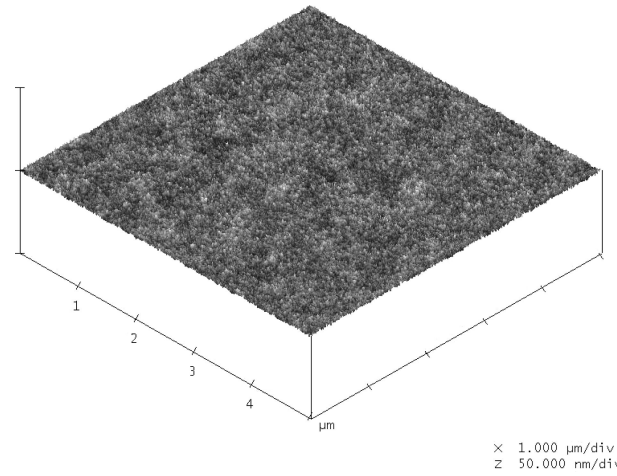

Figure 8. AFM surface profile of a PS−MPTMS/TiO_2 composite film with 27 vol % of TiO_2. Other composition composites have similar surfaces.

Figure 6 shows that the volume average model gives the highest composite index while the serial model predicts the lowest composite index.

It is important to point out how the filler volume affects the composite index in our material system, especially when a molecular composite is formed. We therefore plotted our measured refractive index against that predicted by different models. In determining the volume fraction of the filler, a refractive index of 2.0 and a density of 3.0 g cm^{-3} for amorphous TiO_2 filler and 1.54 and 1.1, respectively, for PS−MPTMS were used. Plotted against the predicted values, our measured composite refractive indices show a parabolic response to the filler volume, well above the predicted range of optical properties. Since all the samples in Figure 7 were examined by TEM and they showed featureless microstructures (see Figure 3c), the cause of this anomaly is not due to a nonuniform distribution of Ti in the polymer matrix. Although the film thicknesses were controlled as similar as possible for all the films, nevertheless it ranged from 1200 to 2200 Å and in general became thinner with more TiO_2 loading. Variation in film thickness also cannot account for the observed optical properties. For example, the measured refractive index at 12.3 vol % TiO_2 is 1.68, and this is higher than the highest predicted value by 0.08. Similarly, at 27 vol % TiO_2 this value is 1.76, also higher than the prediction by 0.08. It is emphasized that the composite coatings all have a smooth surface, and this ensures a good measurement using an ellipsometer. It has a surface roughness of 0.45 nm as measured by AFM (Figure 8). The smooth surface is not unexpected because of the uniform intermixing of these two phases.

The result suggests that the optical behavior of these composites cannot be adequately described using effective medium theories. These models assume that the chemical structure of each constituent is physically independent of each other. Hence, one would not expect effective medium models to hold if the refractive index results from the interaction of light with electrons associated with modified chemical bonds between neighboring constituents formed at the molecular level, especially if the wave function of electrons in the titanium component is modified by its neighboring organic constituent, and vice versa. The detectable chemical bonding between titania and the matrix polymer (by NMR) and the direct imaging of microstructural uniformity at the nanometer level (by TEM) all point to the likelihood that our composite system does not fit the assumptions of effective medium theories.

Alternatively, our results appear better fitted with the molecular refractive index theory, especially the concept of molecular refraction.[50,51] Lorentz and Lorenz formulated the first theoretic correlation between the refractive index and chemical structure:

$$P \equiv R_{LL} = \frac{n^2 - 1}{n^2 + 1} \frac{M}{\rho} \quad (1)$$

where P is the molar polarization, M is the molecular weight, ρ is the density, and n is the refractive index. P is a fundamental

molecular quantity as introduced by Mostotti and Clausius.[52] Quantum mechanics as well as empirical regression had been used to calculate the atomic, group, and bond contribution to the molecular refraction (P or R_{LL} as in eq 1).[53,54] In particular, Goedhart made an extensive regression analysis based on ~1000 compounds containing 43 different functional groups.[55] His value of group contribution of these 43 functional groups to the molecular refraction has been proven to predict well the refractive index based on molecular structure. For example, the benzene ring has a R_{LL} of 25.51, while the methyl group has a R_{LL} of only 5.644 at a 589 nm wavelength. It is our belief that functional group contribution is required to explore the refractive index of molecular composite, such as the one described in this report. The quantum mechanics calculation will be further explored. It is speculated that the bonding of the titanium atom to the polymer chain significantly changes the polarizability of the groups on the polymer chain as well as the local density state. Therefore, the contribution of the nanofiller is more than additivity as predicted by effective medium treatment. Empirically, a parabolic equation describes well the composite index:

$$n_c = -0.4V_{TiO2}{}^2 + 0.78V_{TiO_2} + 1.568 \quad (2)$$

where n_c is the composite refractive index and V_{TiO_2} is the volume fraction of the TiO_2.

Equation 2 can be approximately simplified as

$$n_c = 2.0 - 0.4V_{pol}{}^2 \quad (3)$$

where V_{pol} is the volume fraction of the polymer.

Equation 3 satisfies the boundary condition at 0% filler and 100% filler. It shows that in our formed molecular composite the composite refractive index is strongly influenced by the high index material and diluted by the low index in a slower pace with $V_{pol}{}^2$ rather than linear with V_{pol}, as approximated by the effective medium theories.

Further, eq 3 is generally expressed as

$$n_c = n_{filler} - \Delta n V_{pol}{}^2 \quad (4)$$

where n_{filler} is the refractive index of the high index material and Δn is the index difference between the high and low index material. At present, eq 4 is empirical and based on only one material system. Further work is being pursued to generate molecular composites of different chemical compositions to further test the validity of eq 4 as well as a more rigorous derivation from quantum mechanics.

Conclusion

As discussed in this paper, unique molecular composite films of PS−MPTMS and TiO_2 were formed through a simple *in situ* composite synthesis method. TEM and AFM showed no phase contrast between the organic and inorganic phases. The formation of the molecular composite is believed to be caused by the strong chemical bonding between the polymer chain and the functionalized nano TiO_2. This resulting molecular composite exhibits a refractive index much higher than that predicted on the basis of effective medium theories. Empirical regression of the composite index suggests that the change of the molecular polarizability of the polymer contributes to the synergistic optical property enhancement of the composite.

Acknowledgment. The authors thank Nancy Furbeck, Jill Fornalik, and Theodore VanDam as well as Drs. Brian Antalek and David Bailey for their assistance in copolymer synthesis, composite film preparation, and all of the analytical work. Rao thanks Drs. Xin Jin, Laura Weller-Brophy, Christine Landry-Coltrain, and Edward Schofield for their enlightening discussions and support of the work.

References and Notes

(1) Murray, C. B.; Norris, D. J.; Bawendi, M. G. *J. Am. Chem. Soc.* **1993**, *115*, 8706.
(2) Yoffe, A. D. *Adv. Phys.* **2001**, *50*, 1.
(3) Okada, A.; Usuki, A. *Mater. Sci. Eng.* **1995**, *c3*, 109.
(4) Gehr, R. J.; Boyd, R. W. *Chem. Mater.* **1996**, *8*, 1807.
(5) Zhang, Q.; Wang, J.; Wu, G.; Shen, J.; Buddhudu, S. *Mater. Chem. Phys.* **2001**, *72*, 56.
(6) Ramaswami, R.; Sivarajan, K. *Optical Networks: A Practical Perspective*; Morgan Kaufmann: San Francisco, 2001.
(7) Rockenberger, J.; Scher, E. C.; Alivisatos, A. P. *J. Am. Chem. Soc.* **1999**, *121*, 11595.
(8) Balasubramanian, R.; Kwon, Y.-G.; Wei, A. *J. Mater. Chem.* **2007**, *17*, 105.
(9) Geballe, T. H., Cody, G. C., Sheng, P., Eds. *Physical Phenomena in Granular Materials*; MRS Press: Pittsburgh, 1990.
(10) Lyklema, J. *Fundamentals of Interface and Colloid Science*; Academic Press: New York, 1991; Vol. I.
(11) Brinker, C. J.; Scherer, G. W. *Sol-Gel Science*; Elsevier Science: Amsterdam, 1989.
(12) Livage, J.; Henry, M.; Sanchez, C. *Prog. Solid State Chem.* **1988**, *18*, 259.
(13) Bradley, D. C.; Gaze, R.; Wardlaw, W. *J. Chem. Soc.* **1957**, 469.
(14) Watenpaugh, K.; Caughlan, C. N. *Chem. Commun.* **1967**, 76.
(15) Kulbaba, K.; Manners, I.; Macdonald, P. M. *Macromolecules* **2002**, *35*, 10014.
(16) Aegerter, M. A.; Mennig, M.; Muller, P.; Schmidt, H. *Verre* **2000**, *6*, 30.
(17) Huang, H.-H.; Orler, B.; Wilkes, G. L. *Polym. Bull.* **1985**, *14*, 557.
(18) Li, C.-Y.; Tseng, J. Y.; Morita, K.; Lechner, C.; Hu, Y.; Mackenzie, J. D. *Sol-Gel Optics II. Proc. SPIE* **1992**, *1758*, 410.
(19) Mascia, L. *Trends Polym. Sci.* **1995**, *3*, 61.
(20) Nass, R.; Arpac, E.; Glaubitt, W.; Schmidt, H. *J. Non-Cryst. Solids* **1990**, *121*, 370.
(21) Ravaine, D.; Seminel, A.; Charbouillot, Y.; Vincens, M. *J. Non-Cryst. Solids* **1986**, *82*, 210.
(22) Schmidt, H. *J. Non-Cryst. Solids* **1985**, *73*, 681.
(23) Schottner, G. *Chem. Mater.* **2001**, *13*, 3422.
(24) Coltrain, B. K.; Ferrar, W. T.; Landry, C. J. T.; Molaire, T. R.; Zumbulyadis, N. *Chem. Mater.* **1992**, *4*, 358.
(25) Li, C.; Gu, Y.; Xiaobo, L.; Yaobang, Z.; Anbing, T. *Thin Solid Films* **2006**, *515*, 1872.
(26) Chiang, P.-C.; Whang, W.-T. *Polymer* **2003**, *44*, 2249.
(27) Mauritz, K. A.; Jones, C. K. *J. Appl. Polym. Sci.* **1990**, *40*, 1401.
(28) Lantelme, B.; Dumon, M.; Mai, C.; Pascault, J. P. *J. Non-Cryst. Solids* **1996**, *194*, 63.
(29) Okimura, K. U. *Surf. Coat. Technol.* **2001**, *135*, 286.
(30) O'Regan, B.; Grätzel, M. *Nature (London)* **1991**, *353*, 737.
(31) Takeda, S.; Suzuki, S.; Odaka, H.; Hosono, H. *Thin Solid Films* **2001**, *392*, 338.
(32) Best, M. F.; Condrate, R. A. *J. Mater. Sci. Lett.* **1985**, *4*, 994.
(33) Music, S.; Gotic, M.; Ivanda, M.; Popovic, S.; Turkovic, A.; Trojko, R.; Sekulic, A.; Furic, K. *Mater. Sci. Eng. B* **1997**, *47*, 33.
(34) Terabe, K.; Kato, K.; Miyazaki, H.; Yamaguchi, S.; Imai, A.; Iguchi, Y. *J. Mater. Sci.* **1994**, *29*, 1617.
(35) Arroyo, R.; Cordoba, G.; Padilla, J.; Lara, V. *Mater. Lett.* **2002**, *54*, 397.
(36) Ivanda, M.; Music, S.; Popovic, S.; Gotic, M. *J. Mol. Struct.* **1999**, *480−481*, 645.
(37) Kotani, Y.; Matsuda, A.; Tatsumisago, M.; Minami, T.; Umezawa, T.; Kogure, T. *J. Sol-Gel Sci. Technol.* **2000**, *19*, 585.
(38) Viornery, C.; Chevolot, Y.; Leonard, D.; Aronsson, B. O.; Pechy, P.; Mathieu, H. J.; Descouts, P.; Gratzel, M. *Langmuir* **2002**, *18*, 2582.
(39) Brandrup J., Immergut, E. H., Grulke, E. A., Eds. *Polymer Handbook*; Wiley: New York, 1999.
(40) Garahan, A.; Pilon, L.; Yin, J.; Saxena, I. *J. Appl. Phys.* **2007**, *101*, 014320.
(41) Flaim, T.; Wang, Y.; Mercado, R. *SPIE Proc. Opt. Syst. Design* **2003**.
(42) Garnett, M. *J. C. Philos. Trans. R. Soc. London* **1904**, *203*, 385.
(43) Boyd, R. W. *Nonlinear Optics*; Elsevier: New York, 2003.
(44) Bruggeman, D. A. G. *Ann. Phys. (Leipzig)* **1935**, *24*, 636.
(45) Bottcher, C. J. F. *Theory of Electric Polarisation*; Elsevier: New York, 1952.
(46) Rio, J. A. d.; Zimmerman, R. W.; Dawe, R. A. *Solid State Commun.* **1998**, *106*, 183.
(47) Robles, M.; Taguena-Martinex, J.; Rio, J. A. d. *Thin Solid Films* **1997**, *294*, 320.
(48) Schulz, B. *High Temp. High Press.* **1981**, *13*, 649.

(49) Braun, M. M.; Pilon, L. *Thin Solid Films* **2006**, *496*, 505.
(50) Lorentz, H. A. *Wied. Ann. Phys.* **1880**, *9*, 641.
(51) Lorenz, L. V. *Wied. Ann. Phys.* **1880**, *11*, 70.
(52) Krevelen, D. W. v. *Properties of Polymers*; Elsevier: New York, 1997.
(53) Vogel, A. *J. Chem. Soc.* **1948**, 1833.
(54) Young, J.; Finn, A. *J. Res. Natl. Bur. Stand.* **1940**, *24*, 759.
(55) Goedhart, D. J. Communication Gel Permeation Chromatography International Seminar, Monaco, 1969.

MA800371V